2024 IEEE International Conference on Robotics and Automation (ICRA 2024)
May 13-17, 2024. Yokohama, Japan

Pegasus: a Novel Bio-inspired Quadruped Robot with Underactuated Wheeled-Legged Mechanism*

Yuzhen Pan[1], Rezwan Al Islam Khan[2], Chenyun Zhang[2], Anzheng Zhang[2], Huiliang Shang[2]

Abstract— **This paper presents the design and analysis of Pegasus, a quadrupedal wheeled robot grounded in biomimicry principles. Pegasus offers two distinct motion modes, including a wheeled motion and a hybrid wheeled-legged motion, enabling adaptability across various tasks and environmental conditions. The robot draws inspiration from the joint structures of quadruped animals and incorporates biomimetic features. At the robot's ankle joint, we imitate the articulation of a radius-ulna joint to enhance the wheeled motion's agility. Additionally, we establish comprehensive mathematical models for adaptive dynamics model, providing a robust theoretical foundation for subsequent motion planning and high-precision control. A novel telescopic vehicle mode is also proposed for complex wheel-leg hybrid motion, offering optimized solutions for intricate robot locomotion. Furthermore, we employ parallel underactuated MPC controllers for each leg at the control level, contributing to heightened motion precision and stability. Extensive validation through physical platform experiments highlights the effectiveness and feasibility of the proposed controllers, offering substantial support for real-world applications in robotics.**

I. INTRODUCTION

Most animals have developed complex joint structures over a long evolutionary process, allowing them to move over various terrains. However, legged locomotion control strategies for robots are more complex and have lower movement speed and load capacity than wheeled structures. In contrast, wheeled robots have advantages in a broader range of applications, with higher speed of movement and energy utilization efficiency but with higher requirements for ground leveling. Therefore, the concept of fusing different modes of locomotion has become a novel research direction to compensate for the shortcomings of their respective structures. Wheeled-legged fusion is an emerging development direction for quadruped robots [1] with strong terrain adaptability, efficient walking ability, and relatively simple control.

Typical representatives of quadrupedal robots include the Cheetah robot proposed by MIT [2][3]. The robot handles unexpected terrain disturbances through reactive gait modifications without needing external sensors or prior knowledge of the environment and can achieve walking speeds of up to 4.5 m/s. Unitree's Go robot represents the low-cost quadruped robot [4], with a maximum load weight of 5 kg, walking speed of 0.8 m/s, endurance of about 3-4 hours, and a price of about 2500 USD.

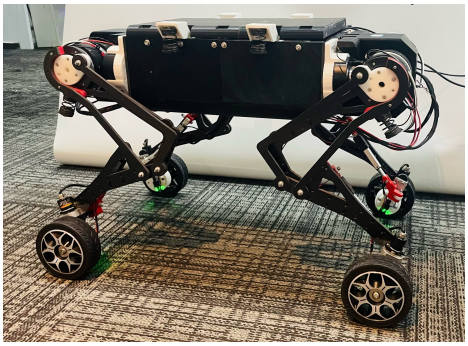

Fig. 1: Pegasus: the bio-inspired wheeled-quadruped robot.

A wheel at the end of the robot is a typical wheeled-legged configuration. One typical example is the Ascento biped wheeled-legged robot. With excellent self-balancing and obstacle-crossing capabilities, the robot can rapidly move over flat terrain and overcome obstacles by jumping. In addition, the ANYmal robot from ETH Zurich [5] is currently at the forefront of this field, possessing a robust adaptive capability that fully utilizes the locomotion advantages of wheeled-legged composite robots over legged robots through innovative motion control and planning techniques. The Italian Polytechnic Institute has proposed a wheel-legged mobile gripping platform, CENTAURO [6]. This robot has dimensions similar to those of a human being and has several manipulators whose platform can carry out demanding operational tasks, and the loads can be considerable.

In order to address the problems of existing robots, such as the inefficient movement of quadruped robots, the poor dynamics model of wheel-legged robots, the optimization of mechanical structure and manufacturing cost, and the lack of bionic analysis, we propose a new robot platform Pegasus in Fig. 1. This paper aims to design and optimize a new quadruped and wheel-legged robot, Pegasus, based on bionic theory, give the corresponding control model and controller, and verify the mechanism parameters and controller scheme through experiments. This robot's mobile platform has two different motion modes, including wheeled and wheeled-legged motion, and has higher adaptability to complex terrain and obstacle-crossing ability.

Section II will focus on analyzing the design concept of the Pegasus robotic system, including its multiple motion modes, the materials used, and the vibration-damping

*This work was supported by the Technology-Driven Agricultural Development Project (Shanghai) under Grant 2022-02-08-00-12-F01128.

[1]Yuzhen Pan is with the School of Academy for Engineering and Technology, Fudan University, Shanghai, China. yzpan21@m.fudan.edu.cn

[2]Rezwan Al Islam Khan, Chenyun Zhang, Anzheng Zhang and Huiliang Shang are with the School of Information Science and Engineering, Fudan University, Shanghai, China. aikrezwan19@fudan.edu.cn, m17701671571@163.com, 13846746728@163.com, shanghl@fudan.edu.cn

Yuzhen Pan and Rezwan Al Islam Khan are co-first authors.

function in the vehicular mode. We also propose a new bio-inspired Ulnar-Radial Joint Mechanism analogous to pronation/supination that can be applied to the wheeled-legged robots while the robot's electronics and software parts are also elaborated. We built the corresponding dynamic models in Section III and proposed the telescopic vehicular model in wheeled mode. Based on the above models, we built the corresponding control system in Section IV. We optimize it with a model predictive control (MPC) controller to improve the robot's motion accuracy and fast response. The corresponding prototype experimental results are also analyzed in this section. Conclusions and future work are discussed and analyzed in Section V.

II. System Overview

A. Mechanics

The robot employs a cost-effective quadrupedal biomimetic design with internal knee joints. Each wheeled-legged module features five degrees of freedom, including hip, thigh, knee, biomimetic ankle joints, and an end-wheel actuator in Fig. 2. The bipedal gait relies on the first three joints, actuated by joint motors with a maximum torque of 30 N·m, ensuring a payload capacity of at least 10 kg. Pegasus, with a weight of 20 kg and dimensions of 50.5 cm $\times$ 70 cm, possesses a height range from 35 cm to 65 cm.

Hip and thigh joint movements are directly actuated in the wheeled-legged mode without linkages. However, the knee joint uses a crank-slider mechanism, simplifying dynamic modeling. The knee joint actuator's low rotational inertia is advantageous for stable control. Carbon fiber is used for solid yet cost-effective links, and finite element analysis ensures controlled deformations. Load-bearing components are made of aluminum alloy, while non-load-bearing parts are 3D printed. The total cost for essential components, including the mechanical structure and actuators, remains under 3000 USD for the whole robot (without onboard computers).

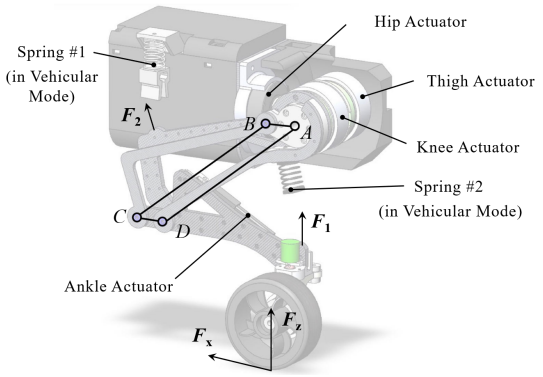

Fig. 2: Mechanical design and configuration of Pegasus.

Additionally, for the Pegasus robot's wheel-based vehicular mode, we introduced shock absorption and suspension systems at the thigh and calf regions, enhancing terrain adaptability. Springs' characteristics are customized based on robot size and weight. During vehicular mode, the robot's weight is distributed onto the shock-absorbing springs, absorbing shock without locking the thigh and knee joint actuators.

Fig. 3: Pegasus in vehicle mode.

B. Bio-inspired Ulnar-Radial Joint Mechanism

Existing wheeled-legged robots typically lack rotational freedom at the ankle joint, restricting the leg's movement to a linear back-and-forth motion. Consequently, controlling such robots requires intricate kinematic algorithms and higher precision, increasing the operation's complexity. Moreover, adding a motor to control the end's rotation would require a powerful torque motor, making the end bulky. These two methods adversely affect the robot's ability to perform complex actions and reduce the leg structure's flexibility.

Here, we observe that the human forearm can achieve both pronation and supination (internal and external rotation) in Fig. 4a. Through literature research [7], we find that this capability lies in the unique configuration of the human forearm, including the proximal and distal radioulnar joints, as well as the humeroradial joint. These joints work in coordination, enabling the forearm to perform pronation and supination movements. In other words, biology has developed a dual-bone forearm structure through evolution, providing the distal end with higher degrees of freedom and flexibility. This design not only exists in humans but is found in nearly all quadruped animals. These two bones allow animals a broader range of flexibility while maintaining joint stability, providing more precise control, which is crucial for enhancing limb function and survival.

We have designed a novel biomimetic ankle joint suitable for wheeled-legged robots in Fig. 4b-d. The main feature of this biomimetic ankle joint is to achieve rotation through a linear actuator, providing precise motion control for the robot. This design's uniqueness lies in applying biomimetic principles, mimicking vertebrates' pronation and supination modes like the radius and ulna bones. The role of the linear actuator simulates the synergistic action of the pronator and supinator muscles. This design enhances the robot's agility and makes the overall device more compact and lightweight, potentially improving the robot's efficiency and applicability. According to the Chebychev–Grübler–Kutzbach formula in (1), for a spatial mechanism with a rigid body's spatial DOF $d = 6$, the number of links $n = 7$, the number of joints $g = 7$, and each joint's degree of freedom $f_i = 1$,

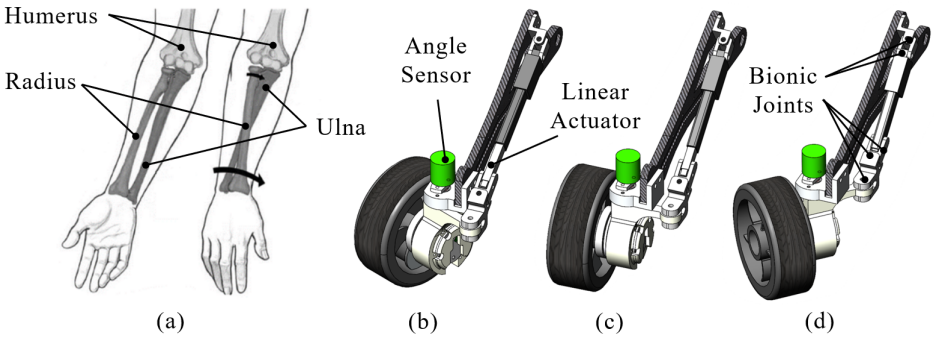

Fig. 4: (a) Radio-ulnar joint of human. (b,c,d) Bionic radio-ulnar joint on Pegasus.

the mechanism's degrees of freedom can be calculated. The result demonstrates the linear actuator's function of operating the wheel's steering direction.

$$M = d\,(n-g-1) + \sum_{i=1}^{g} f_i = 6\times(7-7-1)+7 = 1 \qquad (1)$$

This additional rotational freedom mimics the natural movement of animals. It enables the robot to perform tasks such as stepping over obstacles or adjusting its stance on irregular surfaces, showcasing the practical advantages of biomimetic design principles.

C. Electronics

We use Jetson Orin NX as the host computer, since its powerful arithmetic power can support all the data feedback integration and complex optimization calculations. The arithmetic power allows us to control the overall movement of Pegasus at a frequency of 100Hz. In addition, we have also designed five printed circuit boards (PCB), four of which are used to receive the motor control signals from the host computer and then directly control the joint motor, which slightly increases the transmission time of the control signals. Based on the real-time nature of the microcontroller (MCU), it can significantly improve the robustness of the communication system. The PCB is used to network with the remaining eight motors via the Control Area Network (CAN) and the angle sensor. Angle sensors are used to provide real-time feedback on changes in the steering angle of the bio-inspired joint mechanisms.

D. Software

The software system is realized through the ROS system (C++). Our software system framework is divided into three main parts: 1) keyboard control part, 2) robot control, and 3) communication node for data transmission with the lower computer. The keyboard remote control part sends control commands to the robot, and we can execute different motions according to the different motion modes (e.g., vehicular mode, legged mode, or wheel-legged combination mode) as shown in Fig. 5. Several different gait controllers can be used since ROS2 nodes are simple plug-and-play procedures that can be done during system operation. The communication node is used to communicate with the host computer to give the actual control signals to the motors to make them perform the corresponding motions.

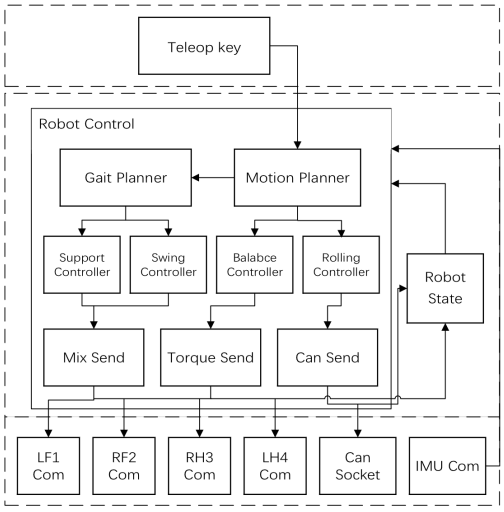

Fig. 5: Software design for Pegasus.

III. Modelling of the Pegasus Robot

Pegasus is an underactuated wheeled-legged robot with additional degrees of freedom from the yaw (bio-inspired ulnar-radial joint mechanism) and wheel mechanism attached to each leg. We have developed two models: a hybrid motion (wheel-legged) model and a pure vehicular model.

A. Preliminary

The generalized coordinates and velocities for the Pegasus torso/body are defined as $\boldsymbol{q}_{\text{torso}} = \left[\boldsymbol{\theta}^{\text{T}}, \boldsymbol{p}^{\text{T}}\right] \in \mathbb{R}^{3+3}$, and $\dot{\boldsymbol{q}}_{\text{torso}} = \left[\boldsymbol{\omega}_{\text{B}}{}^{\text{T}}, \boldsymbol{v}_{\text{B}}^{\text{T}}\right] \in \mathbb{R}^{3+3}$ where $\boldsymbol{v}_{\text{B}}$, $\boldsymbol{\omega}_{\text{B}}$, linear velocity, angular rate in body frame $\mathscr{F}_{\text{B}}$ and $\boldsymbol{p}$, $\boldsymbol{\theta}$ are position, are orientation (in Euler angles) in inertial frame $\mathscr{F}_{\text{N}}$. Each leg of the robot has 5 generalized coordinates $\boldsymbol{q}^{\text{loc}} = \left[\boldsymbol{q}_{\text{j}}^{\text{T}}, \boldsymbol{q}_{\text{ee}}^{\text{T}}\right] \in \mathbb{R}^{3+2}$ and velocities $\dot{\boldsymbol{q}}^{\text{loc}} = \left[\dot{\boldsymbol{q}}_{\text{j}}^{\text{T}}, \dot{\boldsymbol{q}}_{\text{ee}}^{\text{T}}\right] \in \mathbb{R}^{3+2}$ where $\text{loc} \in \{right_{front}, left_{front}, right_{rear}, left_{rear}\}$ joint coordinates $\boldsymbol{q}_{\text{j}} = \left[q_{\text{hip}}, q_{\text{thigh}}, q_{\text{knee}}\right]^{\text{T}}$ and end effector coordinates $\boldsymbol{q}_{\text{ee}} = \left[q_{\text{yaw}}, q_{\text{wheel}}\right]$ in Fig. 6. The reason for splitting the coordinates into two is how dynamic models are defined,

as described in later sections. The combined generalized coordinates and velocities are stacked as follows:

$$\boldsymbol{q} = \left[\boldsymbol{q}_{\text{torso}}, \boldsymbol{q}^{\text{right}_{\text{front}}}, \boldsymbol{q}^{\text{left}_{\text{front}}}, \boldsymbol{q}^{\text{right}_{\text{rear}}}, \boldsymbol{q}^{\text{left}_{\text{rear}}}\right]^{\text{T}} \in \mathbb{R}^{6+5+5+5+5}$$
$$\dot{\boldsymbol{q}} = \left[\dot{\boldsymbol{q}}_{\text{torso}}, \dot{\boldsymbol{q}}^{\text{right}_{\text{front}}}, \dot{\boldsymbol{q}}^{\text{left}_{\text{front}}}, \dot{\boldsymbol{q}}^{\text{right}_{\text{rear}}}, \dot{\boldsymbol{q}}^{\text{left}_{\text{rear}}}\right]^{\text{T}} \in \mathbb{R}^{6+5+5+5+5}$$

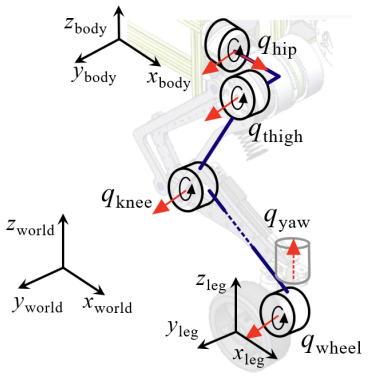

Fig. 6: Modelling and frames of the Pegasus robot.

B. Dynamics Model

Two adaptive dynamic models for whole-body motion will be analyzed in detail. The first one is for hybrid locomotion of the robot, and the second is for pure vehicle mode. The dynamic model for each leg has been modeled separately.

1) Hybrid locomotion: We follow similar modeling techniques described in the literature for underactuated-legged robots. The governing idea behind this centroidal kino-dynamic model is to model the torso as a single rigid body (SRBD) with mass-less kinetic legs. We adopt a similar approach described in [5] to reduce the dimension and constraints of yaw and wheel rotation. The robot's wheel is modeled as a moving point contact, which is rotated and translated onto a rolling direction using corresponding $\boldsymbol{q}_{ee}$ and $\dot{\boldsymbol{q}}_{ee}$ of a leg. The model is simplified by assuming negligible leg joint momentum compared to torso inertia, a constant $\boldsymbol{I}_{nom}$ matrix for some nominal joint configurations. The equations of the motion (EoM) are listed as follows:

$$\dot{\boldsymbol{\theta}} = {}^{\text{N}}\boldsymbol{T}^{\text{B}}(\boldsymbol{\theta})\boldsymbol{\omega}_{\text{B}} \qquad \dot{\boldsymbol{p}} = {}^{\text{N}}\boldsymbol{d}^{\text{B}}(\boldsymbol{\theta})\boldsymbol{v}_{\text{B}} \tag{2a}$$

$$\dot{\boldsymbol{\omega}}_{\text{B}} = \boldsymbol{I}_{\text{nom}}^{-1}\left(-\boldsymbol{\omega}_{\text{B}} \times \boldsymbol{I}_{nom}\boldsymbol{\omega}_{\text{B}} + \sum_{\text{loc}} {}^{\text{B}}\boldsymbol{d}^{\text{E}}(\boldsymbol{q}_j^{\text{loc}}) \times \boldsymbol{F}_{\text{loc}}\right) \tag{2b}$$

$$\dot{\boldsymbol{v}}_{\text{B}} = \boldsymbol{g}(\boldsymbol{\theta}_{\text{B}}) + \frac{1}{m}\sum_{\text{loc}} \boldsymbol{F}_{\text{loc}} \tag{2c}$$

$$\dot{\boldsymbol{q}}_j^{\text{loc}} = \boldsymbol{q}_j^{\text{loc}} \qquad \forall loc \in \{right_{front}, left_{front}, right_{rear}, left_{rear}\} \tag{2d}$$

Here, ${}^{\text{N}}\boldsymbol{T}^{\text{B}}$, ${}^{\text{N}}\boldsymbol{T}^{\text{B}}$ are the transformation matrix for rotation and position from frame $\mathscr{F}_{\text{B}}$ to $\mathscr{F}_{\text{N}}$. Similarly, ${}^{\text{B}}\boldsymbol{d}^{\text{E}}$ is the position matrix $\mathbb{F}_{\text{B}}$ to end effector contact point. $\boldsymbol{F}_{\text{loc}}$ is the contact force acting on it. $\boldsymbol{g}(\boldsymbol{\theta}_{\text{B}})$ is the gravitational acceleration in frame $\mathscr{F}_{\text{B}}$. $\boldsymbol{q}_j^{\text{loc}}$ is the joint configuration input.

2) Telescopic vehicular model: This dynamic model is used when the robot operates in vehicle mode in Fig.3, 7. We are naming it a telescopic vehicle model due to the reconfigurable wheelbase width (front and rear) and base length. The joint coordinates of the robots are mapped into the vehicle dynamic model coordinates using kinematics defined from $\mathscr{F}_{\text{B}}$ to the frame of the corresponding joint coordinates $\in \boldsymbol{q}^{\text{loc}}$. Wheelbase width prismatic joint q_1 is mapped to front right and left q_{hip} in Fig. 6. Similarly, q_2 is mapped to the rear right and left q_{hip}. Base length joint coordinates $q_3 \rightarrow q_6$ is mapped to q_{thigh} and $q_{\text{knee}} \forall_{\text{loc}}$.

Front base length joints q_3, q_4 and rear base length joints q_5, q_6 serve a dual purpose. If controlled in conjunction, the robot changes the length of the vehicle configuration, while individual position configuration will result in an Ackermann-like steering axle configuration. Wheel yaw q_7 is directly (no kinematic transformation) mapped to front right and left q_{yaw}. Similarly, q_8 is mapped to rear q_{yaw} coordinates. Finally, rotations $q_9 \rightarrow q_{12}$ are mapped directly to $q_{wheel} \forall loc$ without any kinematic transformations. $\mathscr{C}_k$, $i \in \mathbb{Z}^+ (i = 1 \sim 4)$ are the frames for the $\mathscr{F}_N$ contact points. These contact points are subject to rolling without slipping nonholonomic constraints, i.e., the velocity of the contact point normal to the x axis is zero.

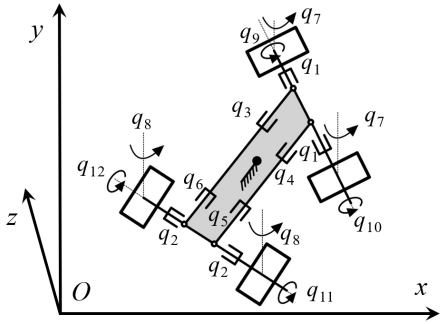

Fig. 7: Telescopic vehicular mode, xy is the ground plane.

For generalized coordinates $\boldsymbol{q}_v = \left[\boldsymbol{\theta}_v, \boldsymbol{p}_v, \boldsymbol{q}_{v_j}\right] \in \mathbb{R}^{3+3+12}$ and velocities $\dot{\boldsymbol{q}}_v = [\boldsymbol{\omega}_{v_B}, \boldsymbol{v}_{v_B}, \dot{q}_{v_j}] \in \mathbb{R}^{3+3+12}$, the rigid body dynamics is given by following:

$$\boldsymbol{M}(\boldsymbol{q}_v)\ddot{\boldsymbol{q}}_v + \boldsymbol{C}(\boldsymbol{q}_v, \dot{\boldsymbol{q}}_v)\dot{\boldsymbol{q}}_v = \boldsymbol{S}^T\boldsymbol{\tau} + \boldsymbol{\tau}_g(\boldsymbol{q}_v) + \sum_{\text{k}=1}^{\text{n}_\text{c}} \boldsymbol{J}_{\mathscr{C}_\text{k}}\boldsymbol{f}_\text{k} \tag{3}$$

Here, $\boldsymbol{M}(\boldsymbol{q}_v)$ and $\boldsymbol{C}(\boldsymbol{q}_v, \dot{\boldsymbol{q}}_v)$ are 18×18 mass and Coriolis matrix. $\boldsymbol{\tau}$ is the actuated torque vector of size 18. The first six entries of this vector are zero due to underactuation. $\boldsymbol{\tau}_g(\boldsymbol{q}_v)$ are external joint torques caused by gravity vector of size 18. $\boldsymbol{S}$ is the selection matrix actuated coordinates. $\boldsymbol{S} = [\boldsymbol{0}_{6\times12}, \boldsymbol{1}_{12\times12}]$. $\text{n}_{\mathscr{C}} = 4$ is the number of contact points; $\boldsymbol{J}_{\mathscr{C}_\text{k}}$ is the contact Jacobian matrix of the position vector in the inertial frame. $\boldsymbol{p}_{\mathscr{C}_\text{k}}(\boldsymbol{q})$ of a contact point $\mathscr{C}_\text{k}$, and $\boldsymbol{f}_\text{k}$ are contact forces exerted by environment on that point. (3) can

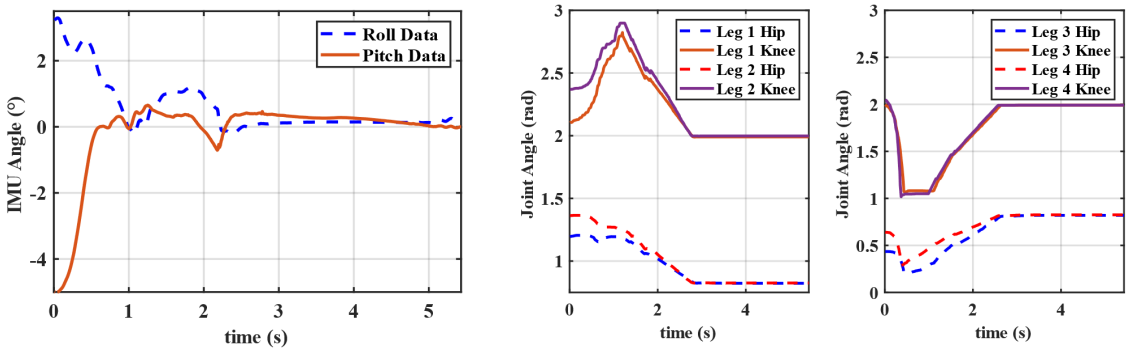

(a) (b) (c)

Fig. 8: Experiment data when the robot is applied with the control system. (a) Roll and Pitch angle data, which stabilize after 2.5s. (b, c) Angle data for each leg's joint.

be written as follows:

$$\dot{\boldsymbol{q}}_v = \boldsymbol{M}(\boldsymbol{q}_v)^{-1}\left(\boldsymbol{S}^{\mathrm{T}}\boldsymbol{\tau} + \boldsymbol{\tau}_g(\boldsymbol{q}_v) - \boldsymbol{M}(\boldsymbol{q}_v)\ddot{\boldsymbol{q}}_v - \boldsymbol{C}(\boldsymbol{q}_v,\dot{\boldsymbol{q}}_v)\dot{\boldsymbol{q}}_v + \sum_{\mathrm{k}=1}^{\mathrm{n_c}} \boldsymbol{J}_{\mathscr{C}_\mathrm{k}}\boldsymbol{f}_\mathrm{k}\right) = f_v(\boldsymbol{q}_v,\dot{\boldsymbol{q}}_v,\ddot{\boldsymbol{q}}_v,\boldsymbol{f},\boldsymbol{\tau}_g) \quad (4)$$

Similar to the dynamic model for hybrid locomotion, the model is simplified with assumptions: zero inertial coupling forces from the joints, i.e. $\boldsymbol{M}(\boldsymbol{q}_v)\ddot{\boldsymbol{q}}_v$ and constant inertia matrix for some nominal joint configuration.

3) Leg Manipulator Model: Due to the control architecture, we have developed a separate dynamic model for all four legs. Each leg's generalized coordinate and velocities are detailed in Section III-A. $\boldsymbol{q}^{\mathrm{loc}}$ and velocities $\dot{\boldsymbol{q}}^{\mathrm{loc}}$ where loc is the leg position. Fig. 6 shows the frame assignment, and the mounting frame is considered fixed with respect to $\mathscr{F}_B$. We use a similar approach described in the previous section to derive the rigid body dynamics for each leg and has same structure like in (3)(4) and formulate the dynamic model function $f_{\mathrm{loc}}(\boldsymbol{q}_v,\dot{\boldsymbol{q}}_v,\ddot{\boldsymbol{q}}_v,\boldsymbol{f},\boldsymbol{\tau}_g)$.

IV. Control System and Experiments

We have deployed six underactuated model predictive controllers (MPC): the model described in Section III-B.1 and Section III-B.2, as well as one for each leg. MPC for hybrid locomotion and vehicle mode optimizes joint coordinates and contact forces and sends the optimized controller action to each leg. The MPC of each leg then uses the optimized joint coordinates and contact forces as reference states and generates optimized torque for each joint for the corresponding leg. In short, the MPC of the legs performs the task of a tracking controller.

A. MPC for Pegasus

To formulate MPC, let us consider a non-linear deterministic dynamic system with state vector $\boldsymbol{x}(t)$ and control input $\boldsymbol{u}(t)$ in the form $\dot{\boldsymbol{x}} = f(\boldsymbol{x}(t),\boldsymbol{u}(t))$. As MPC is an optimal control problem (OCP) and solved using a computer, the system is discretized in the form $\boldsymbol{x}(k+1) = f(\boldsymbol{x}(k),\boldsymbol{u}(k))$. The OCP is given by as follows:

$$\min_{\boldsymbol{u}} J_N(\boldsymbol{x},\boldsymbol{u}) = m(\boldsymbol{x}(N),\boldsymbol{u}(N-1)) + \sum_{k=0}^{N-2} l(\boldsymbol{x}(k),\boldsymbol{u}(k)) \quad (5)$$

$$\text{subject to } \begin{cases} \boldsymbol{x}(k+1) = \boldsymbol{f}(\boldsymbol{x}(k),\boldsymbol{u}(k)) & \boldsymbol{x}(0) = \boldsymbol{x}_0, \\ \boldsymbol{u}(k) \in U, \forall k \in [0,N-1] & \boldsymbol{x}(k) \in X, \forall k \in [0,N] \\ g(\boldsymbol{x}_k,\boldsymbol{u}_k,k) \le 0 & g_{\mathrm{terminal}}(\boldsymbol{x}_{\mathrm{N}}) \le 0 \end{cases} \quad (6)$$

Here, N is the discretized time horizon number steps $N = T/\Delta t$. Running (staging) cost $l(\boldsymbol{x},\boldsymbol{u}) = \|\boldsymbol{x}-\boldsymbol{x}^r\|^2_{\boldsymbol{Q}} + \|\boldsymbol{u}-\boldsymbol{u}^r\|^2_{\boldsymbol{R}}$, and terminal cost $m(\boldsymbol{x}(\mathrm{N}),\boldsymbol{u}(\mathrm{N}-1)) = \|\boldsymbol{x}-\boldsymbol{x}^r\|^2_{\boldsymbol{Q}_{\mathrm{terminal}}} + \|\boldsymbol{u}-\boldsymbol{u}^r\|^2_{\boldsymbol{R}_{\mathrm{terminal}}}$. Matrices $\boldsymbol{Q}$, $\boldsymbol{Q}_{\mathrm{terminal}}$ and $\boldsymbol{R}$, $\boldsymbol{R}_{\mathrm{terminal}}$ are positive semi-definite weight matrices for state $\boldsymbol{x}$ and control input $\boldsymbol{u}$. $\boldsymbol{x}^{\mathrm{r}}$, and $\boldsymbol{u}^{\mathrm{r}}$ are reference state and reference control. $g(\boldsymbol{x}_{\mathrm{k}},\boldsymbol{u}_{\mathrm{k}},\mathrm{k})$, and $g_{\mathrm{terminal}}(\boldsymbol{x}_{\mathrm{N}})$ are the associated nonlinear constraint for the cost function.

The OCP in (5) can be re-arranged as a non-linear programming (NLP) problem and solved using various numeric solvers. There are various methods to formulate an NLP problem; among them are single shooting, multiple shooting, and orthogonal collocation. The reader is encouraged to read more on these methods in [8].

We have adopted the MPC multi-shooting approach for models described in III-B.1 and III-B.2 with the Runga-Kutta-4 discretized system dynamics and orthogonal collocation with Radau quadrature for the model in III-B.3. State and control inputs for system MPC OCP are listed as follows:

$$\begin{aligned} \text{SRBD} &: \boldsymbol{x}(t) = [\boldsymbol{q}_{\mathrm{torso}},\dot{\boldsymbol{q}}_{\mathrm{torso}},\boldsymbol{q}^{\mathrm{loc}}_j],\ \boldsymbol{u}(t) = [\boldsymbol{q}^{\mathrm{loc}}_j,\boldsymbol{F}_{\mathrm{loc}}]\ \forall \mathrm{loc} \\ \text{Vehicle} &: \boldsymbol{x}(t) = \boldsymbol{q}_v,\ \boldsymbol{u}(t) = [\boldsymbol{q}_{v_j},\boldsymbol{f}_{v_j}] \\ \text{Leg} &: \boldsymbol{x}(t) = \boldsymbol{q}_{\mathrm{loc}},\ \boldsymbol{u}(t) = \boldsymbol{\tau}_{\mathrm{loc}} \end{aligned}$$

We have used Sympy [9] physics API to build a symbolic rigid body model and used the built-in support for Lagrange and Kane's method to generate the EoMs for all the models. These EoMs were then exported to CasADi [10]. The MPC OCPs were defined and compiled into shared object files using CasADi symbolic framework to be solved using IPOPT [11] solver. The controllers were deployed to Nvidia Orin Nx and configured to run in parallel. SRBD and vehicle MPC

receive commands from pre-generated state references and send optimized leg joint coordinates to leg MPCs.

B. Performance Tests

In our study, we successfully built the prototype of the Pegasus robot. We chose a relatively long flat surface as the experimental site for the wheeled motion mode and tested the robot's fastest motion speed in this environment, which reached 2.13 m/s. Such speed is higher than CENTAURO's driving speed, 1.6 m/s [6], and ANYmal's walking speed, 1.3 m/s [12], but not as fast as its agile rolling motion 6.1 m/s. We applied the controller to our robot prototype for testing to verify the effectiveness of our robot controller proposed in the previous section. In our experiments, we place slanted wooden blocks in the robot's moving direction of travel to simulate a wheeled-legged motion scenario. Since each joint motor has position information, we could directly read each joint's angle information. In addition, our robot is equipped with IMU sensors to obtain real-time information about the robot's attitude. The update rate of both types of information is 100 Hz. The experimental data are shown in Fig. 8.

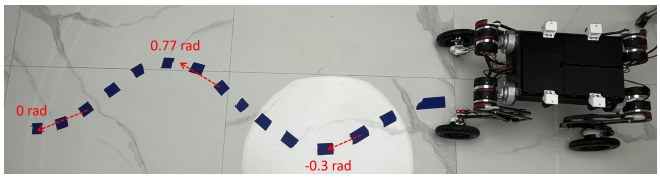

Fig. 9: Vehicular mode test with bio-inspired ankle joints, Pegasus can track the trajectory without legged movement.

Fig. 8a shows the angle information of the robot. We can observe that the robot quickly responded to the obstacle in 0.5 seconds, with subtle vibrations (no more than 1°), and restoring stability in about 2.5 seconds, which verified the feasibility of the controller. According to the graphs in Fig. 8b,c, we can obtain the angle information of each joint. It can be observed that under the external excitation, each joint responds rapidly and dynamically within about 1 second. These experimental results strongly support our study and show that our controller exhibits good performance and feasibility on a real robot. The robot's motion ability and response speed are verified in different environments.

In addition, we designed an S-shaped trajectory to demonstrate the benefits of ankle joints, with the maximum positive and negative deviation angles relative to the starting point indicated in Fig. 9. By controlling the rotation of the wheels through the ankle joints, Pegasus no longer requires legged motion to achieve steering when facing such terrain, which can significantly improve energy efficiency.

V. CONCLUSIONS AND FUTURE WORK

This study introduces Pegasus, a novel quadruped wheeled-legged robot based on biomimicry principles. Pegasus offers a versatile platform capable of two distinct motion modes, enabling adaptability across diverse environments and tasks. Inspired by the joint structures of quadruped animals, Pegasus achieves precise ankle joint control using linear actuators, enhancing its agility. Additionally, establishing comprehensive mathematical models for kinematics and dynamics lays a robust theoretical foundation for subsequent motion planning and high-precision control efforts. The Telescopic vehicle mode motion model and the innovative use of parallel MPC controllers contribute to improved motion accuracy, stability, and flexibility. Extensive validation through physical platform experiments solidifies the effectiveness and feasibility of the proposed novel bio-inspired mechanism and controllers compared to several wheeled-legged robots, affirming the potential for real-world applications in robotics.

Our ongoing research aims to conduct experiments in more complex terrains to enhance the robot's adaptability and obstacle negotiation capabilities. Future research will further evaluate the performance of the novel joint mechanism in more complex terrains to validate and improve its agility and adaptability. Additionally, we will employ more advanced control algorithms like deep reinforced learning to explore various poses and gaits. Lastly, sensor integration, including LiDAR and cameras, will be pursued for enhanced environmental perception to achieve autonomous navigation.

REFERENCES

[1] M. Bjelonic, V. Klemm, J. Lee, and M. Hutter, "A survey of wheeled-legged robots," in *Climbing and Walking Robots Conference*. Springer, 2022, pp. 83–94.

[2] H.-W. Park, S. Park, and S. Kim, "Variable-speed quadrupedal bounding using impulse planning: Untethered high-speed 3d running of mit cheetah 2," in *2015 IEEE International Conference on Robotics and Automation (ICRA)*. IEEE, 2015, pp. 5163–5170.

[3] G. Bledt, M. J. Powell, B. Katz, J. Di Carlo, P. M. Wensing, and S. Kim, "Mit cheetah 3: Design and control of a robust, dynamic quadruped robot," in *2018 IEEE/RSJ International Conference on Intelligent Robots and Systems (IROS)*. IEEE, 2018, pp. 2245–2252.

[4] X. Hu, F. He, and P. Xiao, "Design of a quadruped inspection robot used in substation," in *2021 IEEE 4th Advanced Information Management, Communicates, Electronic and Automation Control Conference (IMCEC)*, vol. 4. IEEE, 2021, pp. 766–769.

[5] M. Bjelonic, R. Grandia, O. Harley, C. Galliard, S. Zimmermann, and M. Hutter, "Whole-body mpc and online gait sequence generation for wheeled-legged robots," *2021 IEEE/RSJ International Conference on Intelligent Robots and Systems (IROS)*, pp. 8388–8395, 2020.

[6] N. Kashiri, L. Baccelliere, L. Muratore, A. Laurenzi, Z. Ren, E. M. Hoffman, M. Kamedula, G. F. Rigano, J. Malzahn, S. Cordasco *et al.*, "Centauro: A hybrid locomotion and high power resilient manipulation platform," *IEEE Robotics and Automation Letters*, vol. 4, no. 2, pp. 1595–1602, 2019.

[7] K. Kawaharazuka, S. Makino, M. Kawamura, Y. Asano, Y. Kakiuchi, K. Okada, and M. Inaba, "Human mimetic forearm design with radioulnar joint using miniature bone-muscle modules and its applications," in *2017 IEEE/RSJ International Conference on Intelligent Robots and Systems (IROS)*. IEEE, 2017, pp. 4956–4962.

[8] L. Wang, *Model Predictive Control System Design and Implementation Using MATLAB*, 1st ed. Springer Publishing Company, 2009.

[9] A. Meurer and C. P. Smith, "Sympy: symbolic computing in python," *PeerJ Computer Science*, vol. 3, p. e103, Jan. 2017.

[10] J. A. E. Andersson, J. Gillis, G. Horn, J. B. Rawlings, and M. Diehl, "CasADi – A software framework for nonlinear optimization and optimal control," *Mathematical Programming Computation*, vol. 11, no. 1, pp. 1–36, 2019.

[11] A. Wächter and L. T. Biegler, "On the implementation of an interior-point filter line-search algorithm for large-scale nonlinear programming," *Mathematical Programming*, vol. 106, no. 1, pp. 25–57, 2006.

[12] C. Weibel, G. Valsecchi, H. Kolvenbach, and M. Hutter, "Towards legged locomotion on steep planetary terrain," in *36th IEEE/RSJ International Conference on Intelligent Robots and Systems (IROS 2023)*, 2023.